Michal A. Brown
Department of Materials Science,
California Institute of Technology,
M/C 205-45,
Pasadena, CA 91125
e-mail: mabrown@Caltech.edu

Tae-Soon Park
Oraxion Diagnostics,
3077 Skyway Court,
Fremont, CA 94539

Ares Rosakis
Graduate Aeronautical Laboratories,
California Institute of Technology,
Pasadena, CA 91125

Ersan Ustundag
Department of Materials Science and
Engineering,
Iowa State University,
2220 Hoover Hall,
Ames, IA 50011

Young Huang
Department of Mechanical Engineering,
University of Illinois at Urbana-Champaign,
Urbana, IL 61801

Nobumichi Tamura

Bryan Valek

Advanced Light Source,
Lawrence Berkeley National Laboratory,
1 Cyclotron Road,
Berkeley, CA 94720

A Comparison of X-Ray Microdiffraction and Coherent Gradient Sensing in Measuring Discontinuous Curvatures in Thin Film: Substrate Systems

The coherent gradient sensor (CGS) is a shearing interferometer which has been proposed for the rapid, full-field measurement of deformation states (slopes and curvatures) in thin film-wafer substrate systems, and for the subsequent inference of stresses in the thin films. This approach needs to be verified using a more well-established but time-consuming grain orientation and stress measurement tool, X-ray microdiffraction (XRD). Both CGS and XRD are used to measure the deformation state of the same W film/Si wafer at room temperature. CGS provides a global, wafer-level measurement of slopes while XRD provides a local micromeasurement of lattice rotations. An extreme case of a circular Si wafer with a circular W film island in its center is used because of the presence of discontinuous system curvatures across the wafer. The results are also compared with a theoretical model based on elastic plate analysis of the axisymmetric biomaterial film-substrate system. Slope and curvature measurements by XRD and by CGS compare very well with each other and with theory. The favorable comparison demonstrates that wafer-level CGS metrology provides a quick and accurate alternative to other measurements. It also demonstrates the accuracy of plate theory in modeling thin film-substrate systems, even in the presence of curvature discontinuities
[DOI: 10.1115/1.2150500]

Introduction and Motivation

As the semiconductor industry develops ever smaller dimensions of thin metal film interconnections and more complex multilayered (film stack) structures, the mechanical properties and stresses of thin films used for these structures become major factors in controlling the reliability of integrated circuits (ICs). However, due to the small size of features of modern ICs, the only way to measure their stresses directly is using X-ray microdiffraction (XRD) since spot sizes are now becoming available at comparable dimensions to such features (e.g., 1 μm and below). At the same time, it is impractical (very time-consuming and costly) to routinely perform many X-ray studies across large areas on a wafer.

Therefore, it is desirable to develop another technique that can yield quick and full-field information regarding the stress state in film structures deposited on wafers, ideally to be used as a quality control tool. A recent optical method developed by Rosakis and co-workers at Caltech has been proposed for this purpose [1–3].

Called coherent gradient sensing (CGS), this technique employs an expanded laser beam to measure all components of the curvature tensor field in thin film-substrate systems. It does so in full-field and produces curvature component maps across the surface of the entire wafer. CGS is insensitive to rigid-body motions, such as those induced by vibration, and is quite suitable for in situ studies. As such, it is ideal for quick, full-field measurements of macro stresses across a wafer surface and can easily be used in quality control. It is further desirable, however, to attain stress state information at the level of individual features in a microelectronic circuit. In this context, Rosakis at Caltech, Suresh at MIT and their co-workers [4–7] have developed sophisticated micromechanical models that relate the data obtained from CGS (macro stresses) to local (micro) stresses in circuits.

In this article, we first describe the CGS and XRD techniques, and then begin the process of validating the CGS methodology.
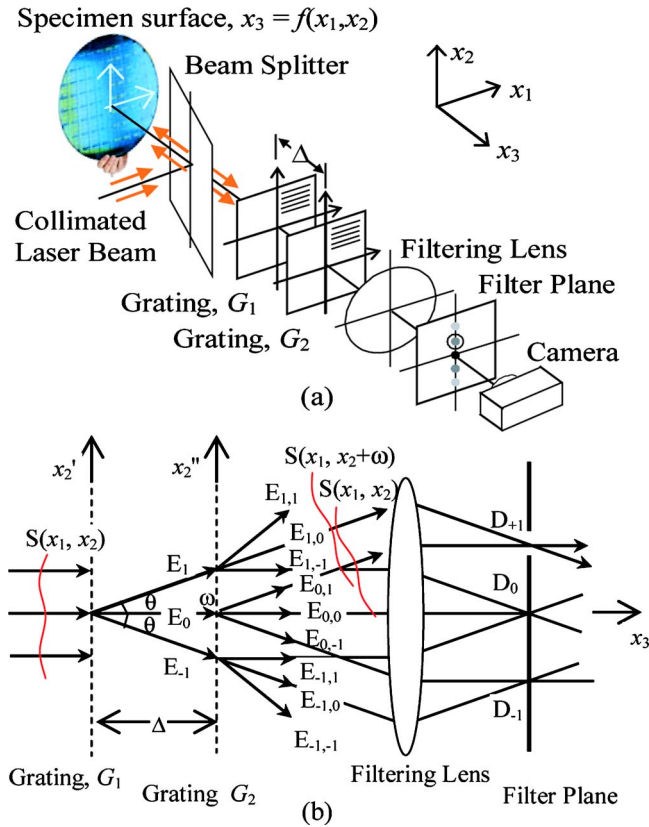
Specimen surface, $x_3 = f(x_1,x_2)$

Fig. 1 Schematic of the CGS setup in reflection mode (*a*) and its working principle (*b*)

The first step, described here, is to compare curvature measurements made with both techniques on specimens with relatively simple features. In the present experiment, a sample consisting of a circular W thin film island deposited on a much thicker circular Si substrate is used. This radially symmetric geometry is particularly interesting because the discontinuous film thickness causes severe discontinuities in system curvatures across the island perimeter, which must be captured by both techniques for accurate measurement and comparison. Since the sample is circular, the bare Si portion has its own curvature which also must be measured. This sample is an excellent test specimen due to its radial geometry, large curvatures, and severe curvature discontinuities that develop because of the partial coverage of the Si substrate by the circular island. The radial symmetry of the system is also amenable to analytical treatment. Indeed an analysis of the relation between film stress and system deformations (slopes, curvatures) is possible based on plate analysis of the thin film-substrate system [8].

Coherent Gradient Sensing (CGS)

The coherent gradient sensing (CGS) method is a self-referencing interferometric technique that produces fringe patterns of surface slope by laterally shearing an initially planar wave front which has been reflected from a specimen (wafer). Figure 1(*a*) shows a schematic of the CGS setup in reflection [1–3]. A coherent, collimated laser beam (300 mm or less in diameter) is directed to a reflecting wafer surface via a beam splitter. In general, the wafer is nonplanar and its surface distortion can be described by the equation $x_3 = f(x_1,x_2)$. The beam reflected from the wafer is also distorted by the nonplanar shape of the wafer. The resulting wave form is described by a two-dimensional surface in space whose equation is given by $x_3 = S(x_1,x_2)$, where $S(x_1,x_2) = 2f(x_1,x_2)$. This distorted wave front is again passed through the

beam splitter and is then incident upon a pair of identical high-density gratings, G_1 and G_2, separated by a distance Δ. The gratings act to optically "shear" or "differentiate" the incident wave front to produce a series of diffracted beams. These beams are separated using a filtering lens to form distinct diffraction spots on a filter plane. An aperture placed in this plane serves to isolate the diffraction order of interest, which is then imaged onto the photographic film plane. For present purposes, either of the ± 1 diffraction orders is of interest, as will be clear in the following discussion.

Figure 1(*b*) is a two-dimensional schematic illustrating the principles of the CGS method. The figure shows the distorted optical wave front, $S(x_1,x_2)$, incident on the two gratings in which the lines are taken to be oriented along x_1. At the first grating, G_1, the incident wave front is diffracted into several wave fronts, $E_0, E_1, E_{-1}, E_2, E_{-2}$, etc., of which only the first three are drawn in Fig. 1(*b*). Each of these wave fronts, in turn, is diffracted by the second grating, G_2, to generate additional wave fronts, such as $E_{0,0}, E_{0,1}, E_{0,-1}$, etc. The diffracted beams are combined by a filtering lens to produce diffraction spots, such as D_0, D_{+1}, D_{-1}, etc., in the focal plane of lens (filter plane). One of the diffraction spots, typically the first diffraction order, the D_{+1} spot, is chosen with an aperture for imaging onto the film plane.

The presence of the two gratings in the path of the optical wave front generates a lateral shift (or shearing) of the wave front. For example, the diffracted beam $E_{1,0}$, whose wave front is denoted as $S(x_1,x_2+\omega)$, is shifted from the beam $E_{0,1}$, whose wave front is denoted as $S(x_1,x_2)$, by a distance ω in the x_2 direction. The shift distance, ω, is expressed as $\Delta \tan \theta$, where $\theta = \arcsin(\lambda/p)$ is the diffraction angle and λ and p are the wavelength of light and the pitch of the gratings, respectively. For small angles of diffraction, $\omega \approx \Delta \theta \approx \Delta(\lambda/p)$, the condition for constructive interference of the original and shifted wave fronts is given by

$$S(x_1,x_2+\omega) - S(x_1,x_2) = n^{(2)}\lambda \quad n^{(2)} = 0, \pm 1, \pm 2, \dots \quad (1)$$

where $n^{(2)}$ is an integer that represents fringes associated with shearing along the x_2 direction. By dividing Eq. (1) by ω, taking ω to be sufficiently small, and substituting $\omega = \Delta(\lambda/p)$, it is seen that

$$\frac{\partial S(x_1,x_2)}{\partial x_2} = \frac{n^{(2)}\lambda}{\omega} = \frac{n^{(2)}p}{\Delta} \quad n^{(2)} = 0, \pm 1, \pm 2, \dots \quad (2)$$

Recalling that $S = 2f$ and repeating the above-presented analysis for gratings aligned along the x_2 direction, it can be shown that the alternating dark and bright interference fringes correspond to constant values of components of the in-plane gradient of the wafer surface topography as follows:

$$\frac{\partial f(x_1,x_2)}{\partial x_\alpha} = \frac{n^{(\alpha)}p}{2\Delta} \quad n^{(\alpha)} = 0, \pm 1, \pm 2, \dots \quad (3)$$

where $\alpha, \beta \in \{1,2\}$. A relative rotation of the gratings to the wafer allows for both orthogonal components of slope to be recorded in the form of full-field slope maps. The three independent components of curvature tensor field, $\kappa_{\alpha\beta}$, can now be determined directly from two orthogonal CGS slope maps by partial differentiation along the x_1 and x_2 directions

$$\kappa_{\alpha\beta}(x_1,x_2) \approx \frac{\partial^2 f(x_1,x_2)}{\partial x_\alpha \partial x_\beta} \approx \frac{p}{2\Delta}\left\{\frac{\partial n^{(\alpha)}(x_1,x_2)}{\partial x_\beta}\right\} \quad (4)$$

In order to determine the full curvature tensor, the gradient fields in two orthogonal directions must be recorded. Equation (4), which applies to the shear (or twist) curvature component, κ_{12}, as well as the normal curvature components, κ_{11} and κ_{22}, is the equation governing the curvature tensor field at any in-plane location (x_1,x_2). It enables the global, full-field measurement of curvature for the film-substrate system. For thin film-thick substrate systems the full-field recording of all system curvature components is crucial since they can be related to the individual components of
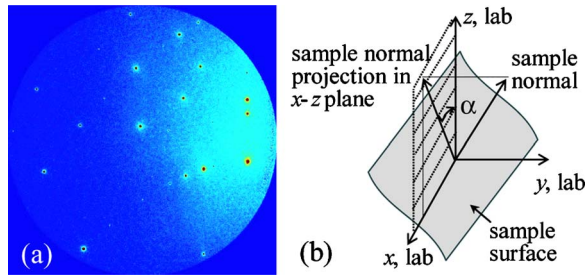
Fig. 2 (*a*) Laue pattern from the single crystal Si wafer. (*b*) Definition of coordinate system and the projection angle α; slope in *xz* plane=tan(α).
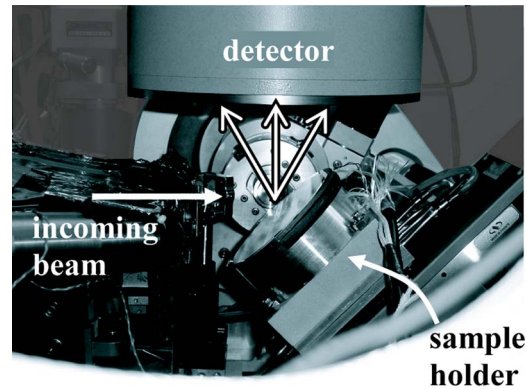

Fig. 3 The microdiffraction setup at the Advanced Light Source. The incoming X-ray beam is reflected from the sample surface and captured by the detector.

stress acting on the thin film, through simple plate theory [4–7]. This provides an easy and quick way of film stress measurement that can be instantaneously performed across an entire wafer surface.

X-Ray Microdiffraction (XRD)

X-ray microdiffraction is a local measurement technique which, in general, uses the lattice spacing in a crystalline structure as a local micro-strain gauge. The incoming beam diffracts from the crystalline lattice to form Laue patterns, which can be analyzed to measure the sample strain and stress. Synchrotron radiation, which was used in this experiment, has several advantages over traditional, commercially available laboratory-grade X-ray machines. These include its very small beam size ($\sim 1 \times 1$ μm), higher energy, and ability to use a polychromatic (white) X-ray beam. In contrast, most lab X-ray machines feature large, monochromatic beam spot sizes of more than 100×100 μm and are thus unable to resolve spatial stress occurring in thin film structures. Also, while a polychromatic beam is used to determine the orientation and 3D deviatoric strain of each grain illuminated, a monochromatic beam takes an average measurement over all diffracting grains.

Laue patterns from a white beam form Laue spots (Fig. 2(*a*)), where each spot is generated by a specific X-ray energy selected by the given lattice plane. A sophisticated software program then deconvolutes these patterns and indexes them, identifying individual patterns from each grain [9]. From this analysis, one can determine the orientation matrix of each grain as well as its deviatoric strain. (The deviatoric stress is then found using Hooke's law [10].) When there are too many grains in an image, the software is unable to determine which spots correspond to which grains, and cannot analyze the image. Therefore, white x rays are used when the grain size is comparable to or larger than the beam size.

In the case of a single crystal specimen, the orientation matrix measured is always from the same grain. Once the crystal orientation is obtained at each location across the specimen, the relative slope and curvature are then determined by tracking the changes in the vector defining the grain normal with respect to the lab coordinate system. For a scan along the *x* axis (sample diameter), we are only concerned with the slope changes in the *xz* plane. This slope is equal to tan(α), where α is defined as the angle between the projection of the grain normal in the *xz* plane and the *z* axis in the lab reference frame (Fig. 2(*b*)).

For a radially symmetric sample on which the scan is performed along the diameter, where *y*=0, cylindrical coordinates can be used. The radial slope, $\partial f / \partial r = \tan(\alpha)$, and the circumferential curvatures κ_{rr} and $\kappa_{\theta\theta}$ are then determined from

$$\kappa_{rr} = \frac{\partial^2 f}{\partial r^2} = \frac{\partial (\tan \alpha)}{\partial r} \qquad (5)$$

$$\kappa_{\theta\theta} = \frac{1}{r} \frac{\partial f}{\partial r} = \frac{1}{r}(\tan \alpha). \qquad (6)$$

The experiment described here was performed at beamline 7.3.3 at the Advanced Light Source (ALS) at Lawrence Berkeley National Laboratory in Berkeley, CA. At this beamline we can measure curvature and strain in the silicon substrate, as well as strain in thin films [9]. The reflection X-ray setup is shown in Fig. 3. In this experiment, white X-rays were used to measure the grain normal orientation across the sample.

Experiments

The same sample was used for both CGS and XRD measurements. This sample consisted of a 2-μm-thick, 25-mm-diam circular W film island in the center of a 100-mm-diam, 525-μm-thick Si 001 wafer (Fig. 4). The Young's modulus for Si and W are, respectively, 130 and 410 GPa, and the Poisson's ratio is 0.28 for both materials [11].

Both CGS and XRD data were collected at room temperature. Using the CGS method, slope, curvature, and stress maps of the sample were obtained in advance. At ALS, pointwise XRD measurements were made along almost the full diameter of the sample, 94.5 mm, with a 0.1 mm step size, yielding the single-crystal Si grain orientation at each point.

As discussed earlier, the geometry of the film-substrate system was chosen in such a way as to feature severe slope and curvature gradients across the wafer in the form of curvature discontinuities occurring at the edge of the film island. It was felt that the accurate recording of curvature jumps across such discontinuities will provide a test for validating CGS metrology through comparison to XRD. The spatial resolution of the XRD measurements (order of 1 μm) was definitely enough to cope with the abrupt spatial variations anticipated. Moreover, the geometry was intentionally kept simple enough so as to allow for straightforward scientific interpretation of the results. Furthermore, it was chosen in such a way as to allow for the development of closed-form analytical relations describing the substrate deformation. The direct comparison of the results of the two measurements with the results of
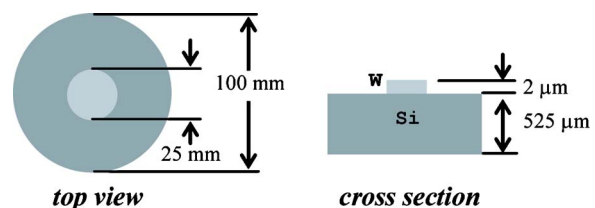

Fig. 4 Sample schematic

the analysis was anticipated to provide further guidance on the interpretation of the measured behavior and to shed light on the ability of elastic plate theory to analyze film-substrate systems which feature discontinuous film geometries.

Theoretical Predictions

The axisymmetric nature of the film substrate system allows for elastic plate theory and the thin film approximation to relate the system curvature fields to the stress in the circular island film. The theoretical development, whose details will be presented elsewhere [8], considers a circular film of thickness h_f and radius R_f deposited in the center of a circular substrate of thickness h_s and radius R_s. The film thickness is much smaller than that of the substrate ($h_f \ll h_s$). The Young's moduli of the film and the substrate are denoted by E_f and E_s, respectively, while their Poisson's ratios are denoted by ν_f and ν_s.

The analysis considers the special case in which both film and substrate are composed of isotropic linear elastic solids, characterized by the above-noted moduli. It is further assumed that the film features an in-plane isotropic, or equibiaxial, stress state characterized by a film stress σ_f such that $\sigma_{xx} = \sigma_{yy} = \sigma_f$ and $\sigma_{zz} = 0$ in any proper orthogonal coordinate frame such that the x and y axes lie on the plane of the film (or the wafer). Alternatively, if a polar coordinate system centered at the island center is used, this is equivalent to $\sigma_{rr} = \sigma_{\theta\theta} = \sigma_f$ where σ_{rr} and $\sigma_{\theta\theta}$ are the radial and circumferential stress components, respectively. Perhaps the most severe restriction of the analysis is that stresses are not allowed to vary across the film (i.e., $\partial \sigma_f / \partial r = 0$) and are restricted to remain spatially constant.

Under the above-mentioned assumptions an elastic boundary value problem can be formulated which relates the radially varying system curvatures to the constant and equibiaxial film stress σ_f. Because of the system's radial symmetry, the only nonzero component of the slope vector is $\partial f / \partial r$ while the only nonvanishing components of the curvature tensor are $\kappa_{rr} = \partial^2 f / \partial r^2$ and $\kappa_{\theta\theta} = (\partial f / \partial r)/r$, the radial and circumferential curvatures, respectively. Axisymmetry requires that the twist curvature component $\kappa_{r\theta}$ vanishes throughout the system.

The analysis shows that the sample curvature within the film-covered region is spatially constant and equibiaxial, i.e., $\kappa_{rr} = \kappa_{\theta\theta} = \kappa$, where κ is independent of the radial position r. In this region the sample curvatures are given by

$$\kappa_{rr} = \kappa_{\theta\theta} = \kappa = \frac{6 h_f \sigma_f (1 - \nu_s)}{E_s h_s^2} \left[1 - \frac{1 - \nu_s}{2} \left(1 - \frac{R_f^2}{R_s^2} \right) \right]$$

$$0 \le |r| \le |R_f| \tag{7}$$

In this region the system deforms as a sphere. It should be noted that for $R_f = R_s$ (full film coverage of the wafer) Eq. (7) coincides with the predictions of the well-known Stoney formula [12] which relates constant film stress to constant system curvatures as described in Ref. [4]. This is an anticipated limiting behavior.

Outside the film covered region, however, the predictions are quite unexpected. Here the system curvatures κ_{rr} and $\kappa_{\theta\theta}$ are not equal and are strong functions of the radial position r. Despite the fact that this region is not covered by the film, its curvature components are nonzero and their magnitude depends on the magnitude of the stress of the film island as

$$\kappa_{rr} = \frac{\partial^2 f}{\partial r^2} = \kappa \frac{1 - \dfrac{1 + \nu_s}{1 - \nu_s} \dfrac{R_s^2}{r^2}}{1 + \dfrac{1 + \nu_s}{1 - \nu_s} \dfrac{R_s^2}{R_f^2}} \quad \kappa_{\theta\theta} = \frac{1}{r} \frac{\partial f}{\partial r} = \kappa \frac{1 + \dfrac{1 + \nu_s}{1 - \nu_s} \dfrac{R_s^2}{r^2}}{1 + \dfrac{1 + \nu_s}{1 - \nu_s} \dfrac{R_s^2}{R_f^2}}$$

$$|R_f| \le |r| \le |R_s| \tag{8}$$

What is also remarkable is that comparison of the expressions for κ_{rr} from within and outside the film-covered region reveals a fi-
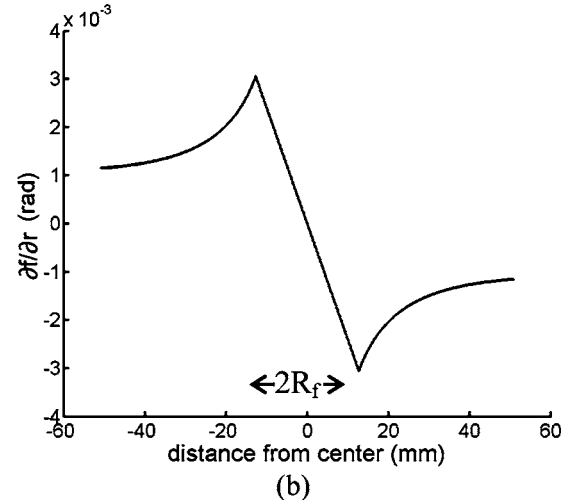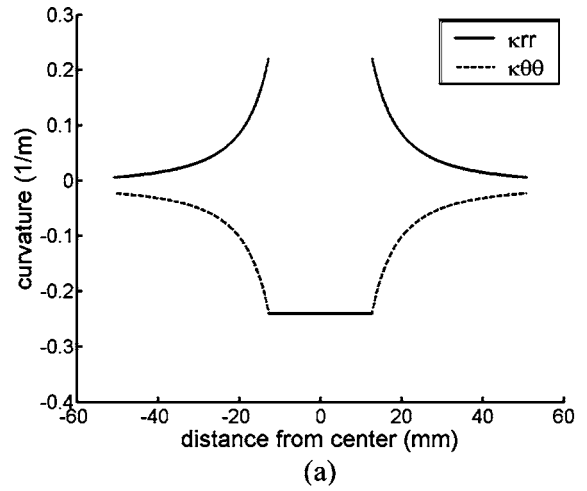

(a)

(b)

Fig. 5 Theoretical prediction of surface (*a*) curvature and (*b*) slope across the diameter of a radially symmetric circular wafer with a circular film island in the center. The assumed film stress is –2 GPa.

nite jump in radial curvature which involves a change of curvature sign across the circular interface $r = R_f$.

The radial slope component $\partial f / \partial r$ can now be computed from Eqs. (7) and (8) and is given by the following relations for the two regions:

$$\frac{\partial f}{\partial r} = \kappa_{\theta\theta} r = \kappa_{rr} r = \kappa r \quad 0 \le |r| \le |R_f| \tag{9}$$

$$\frac{\partial f}{\partial r} = \kappa_{\theta\theta} r = \kappa \frac{1 + \dfrac{1 + \nu_s}{1 - \nu_s} \dfrac{R_s^2}{r^2}}{1 + \dfrac{1 + \nu_s}{1 - \nu_s} \dfrac{R_s^2}{R_f^2}} r \quad |R_f| \le |r| \le |R_s| \tag{10}$$

Within the film-covered region, there is a linear variation of slope with position while the variation of slope outside the film-covered region is more complex. At the interface $r = R_f$, the slopes are, as expected, continuous. Figure 5 shows the predicted variation of the two nonzero curvature components and the radial slope component. The figure is plotted by using the geometry and material parameters of the above-described W-Si system and an assumed film stress, σ_f, of −1.5 GPa. The above-discussed theoretically predicted features are obvious from the figure.
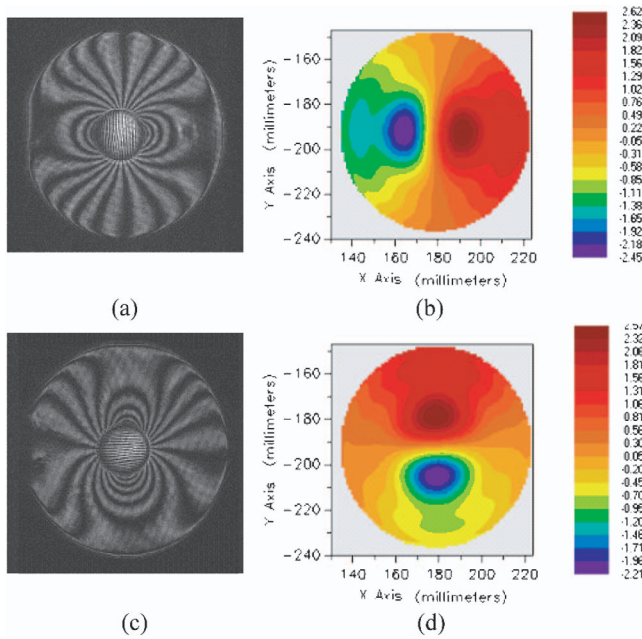
Fig. 6 CGS slope measurements in the *x* and *y* directions. Horizontal, $\partial f/\partial x$: (*a*) wafer image and (*b*) horizontal slope map. Vertical, $\partial f/\partial y$: (*c*) wafer image and (*d*) vertical slope map.

Fig. 7 Wafer topography, through integration of *x* and *y* slope maps: (*a*) full-field map; (*b*) radial cut through *y*=0

Results and Discussion

By using CGS interferometry, the same sample was measured to obtain slope interferograms and digitized full-field slope maps in the *x* and *y* directions (Fig. 6). Since these are in Cartesian coordinates, only the data along the diameters, the extracted linear data set from these maps, can be directly converted to radial slopes. It is worth noting that the Cartesian slope maps in each orthogonal direction differ by only a 90 deg rotation, as is expected for a radially symmetric sample.

The film island is distinctly visible on the *x* and *y* interferograms (Figs. 6(*a*) and 6(*c*)) as a circle in the middle of the picture. The fringe pattern in that region consists of dense, straight, evenly spaced lines that correspond to a constant equibiaxial curvature, as predicted by the analysis. Outside the film island, there is still a less dense but more complex fringe pattern, since there is a non-zero curvature in that area due to the circumferential constraints on the Si wafer. This is also qualitatively consistent with the analysis.

Further image analysis can at this point proceed in two ways—either to the wafer shape, through integration of the slope maps, or to curvature maps, through differentiation of slope components. Integration of the slope maps yields the surface topography of the wafer, as shown in Fig. 7. Consistent with theory (Fig. 5), the sign of the radial curvature component κ_{rr} changes across the film edge. The film region has a negative, constant curvature; there is a jump in curvature from negative to positive at the film edge; and there is a nonzero curvature outside the film.

The slope maps can also be used to calculate the two direct (κ_{xx} and κ_{yy}) and the twist (κ_{xy}) Cartesian curvature maps (Fig. 8). Again, the *x* and *y* curvature maps are very similar, with the noticeable difference being due to the graph color scale. Also note the diagonal symmetry in the twist curvature map. Both of these indicate a radially symmetric curvature state, as expected from the radial sample geometry.

The radial symmetry is verified by calculating the maximum, principal curvature map (Fig. 8(*d*)) by using the following relation [3]:
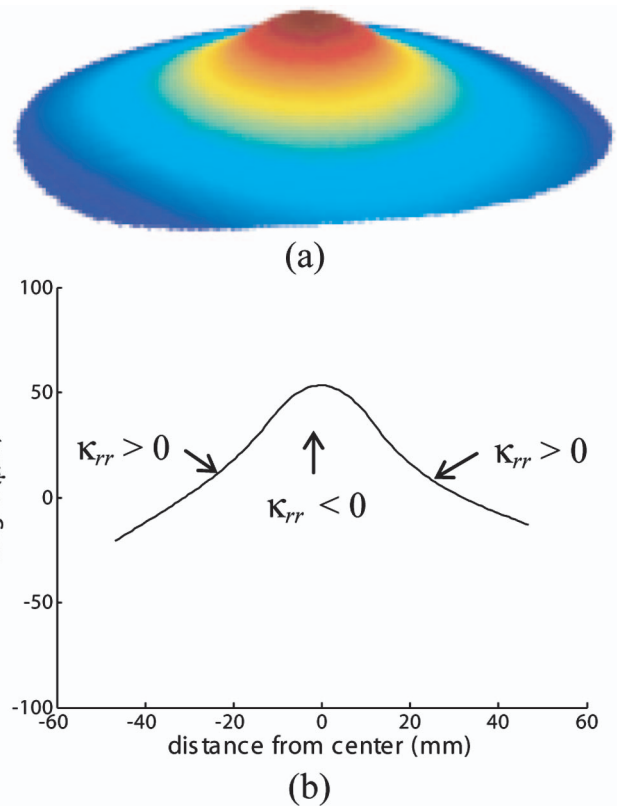
$$\kappa_{max} = \left(\frac{\kappa_{xx} + \kappa_{yy}}{2}\right) + \frac{1}{2}\sqrt{(\kappa_{xx} - \kappa_{yy})^2 + 4\kappa_{xy}^2} \qquad (11)$$

The obvious radial symmetry of this map shows that the axisymmetry assumption of the theory is relevant in this case and implies that $\kappa_{max} = \kappa_{rr}$.

In order to obtain curvature by differentiation of the slope maps, the data are fit to a polynomial function by a numerical analysis. This polynomial fitting uses Zernike polynomials, a fifth-order polynomial set with 37 terms. While originally de-
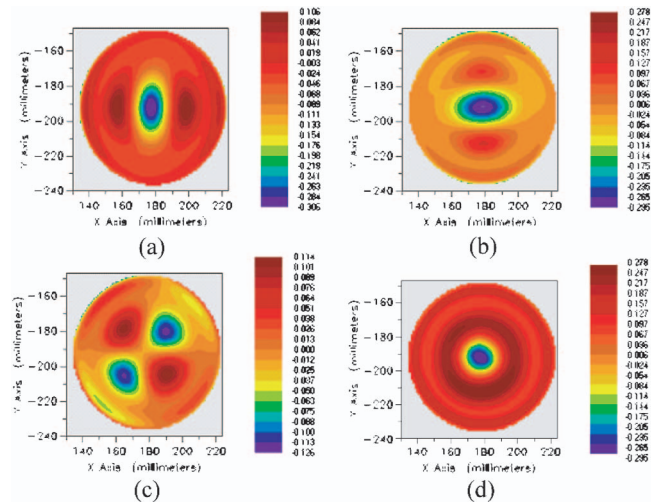

Fig. 8 CGS curvature maps in the *x*, *y* and twist directions: (*a*) horizontal map, $\kappa_{xx} = \partial^2 f/\partial x^2$, (*b*) vertical map, $\kappa_{yy} = \partial^2 f/\partial y^2$, (*c*) twist map, $\kappa_{xy} = \partial^2 f/\partial x\partial y$, (*d*) principal curvature, $\kappa_{max} = \kappa_{rr}$
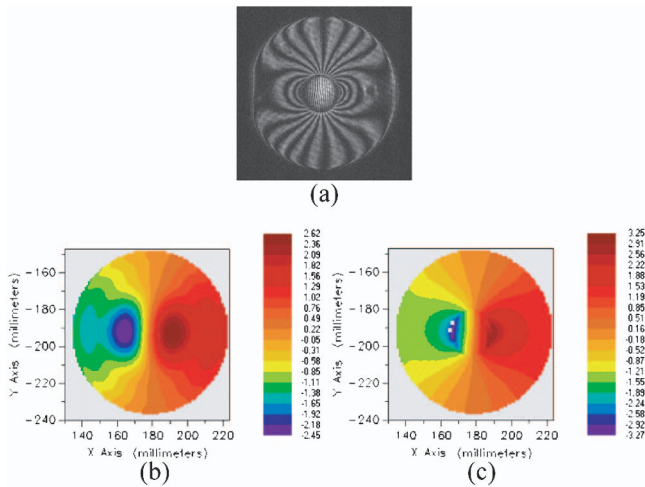
Fig. 9 (*a*) **Horizontal interferogram and slope maps:** (*b*) **with filtering and smoothing and** (*c*) **with no smoothing (raw data)**

signed to characterize optical aberrations, this polynomial set is often used to describe aspheric surfaces from interferometric data. In most cases, where spatial variations of curvature are gradual, this fitting process is advantageous since it filters out noise and allows numerical differentiation to be performed. This particular sample, however, has a highly nonuniform geometry, which corresponds to unusually high gradients in slope and jumps in curvature which are lost in the numerical smoothing process. Gradients in slope this large are not typically seen in modern industrial thin
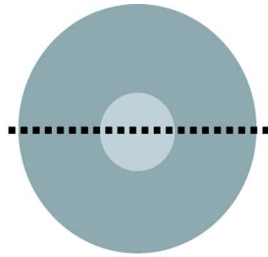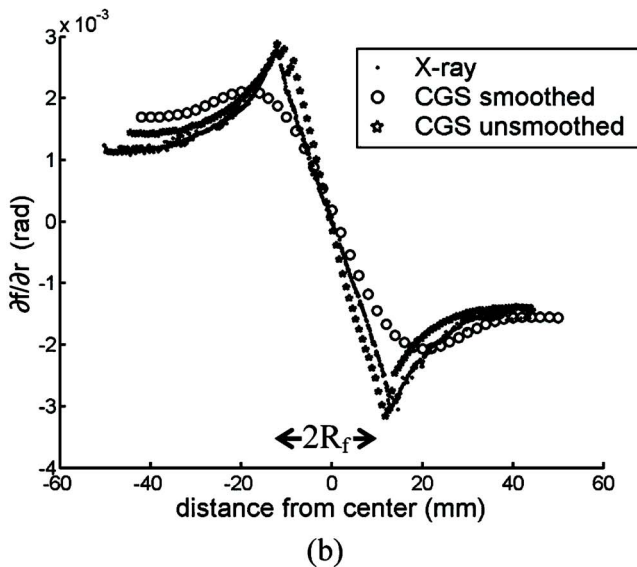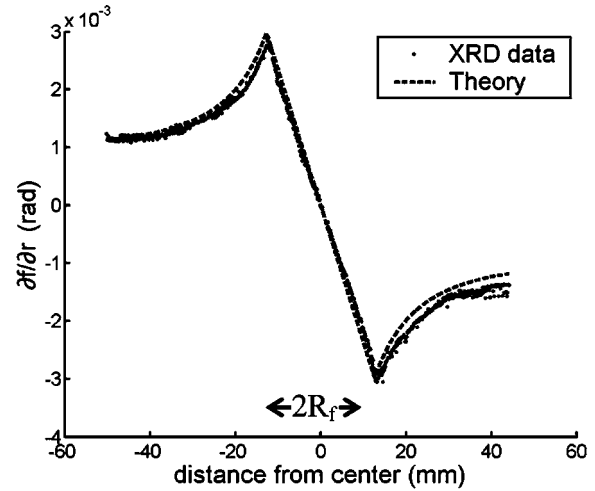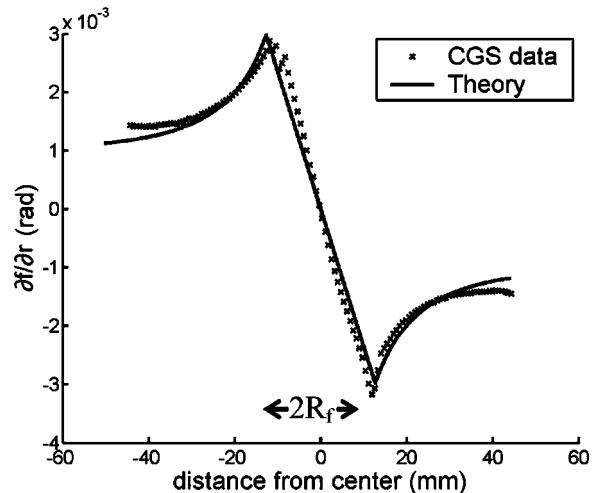

Fig. 10 **Data were extracted from CGS slope maps across the sample diameter** (*a*) **and compared with XRD** (*b*)

Fig. 11 **Comparison of** (*a*) **XRD and** (*b*) **CGS data with theoretical predictions, using film stress as the fitting parameter**

film-substrate systems, which feature small, closely spaced features, and therefore this over-smoothing situation does not, in practice, generally occur.

In this case, the film-covered region should have a constant curvature, or linear slope, which corresponds with straight, evenly spaced vertical lines on the horizontal slope map (Fig. 9). There should also be a sharp transition between the slope of the film covered and that of the bare Si regions. Instead, Fig. 9(*b*) features only approximately vertical lines in the film-covered regions, and only a gradual change to the bare Si region. To circumvent this problem, the numerical smoothing was artificially removed and the resulting unsmoothed digital slope map is displayed in Fig. 9(*c*). In this figure (with no filtering or smoothing), the anticipated straight evenly spaced lines within the film are clearly visible. The sharp transition between the constant and varying curvature inside and outside the film is also recorded. In fact, the film-covered circular island can be easily traced out on this map.

In order to directly compare CGS slope measurements with the XRD data taken along the sample diameter, a linear data set, also selected across the same diameter of the sample (Fig. 10(*a*)), was extracted from both slope maps in Fig. 6. Figure 10(*b*) shows the difference between the smoothed and unsmoothed CGS data, compared with XRD across the same region. In both the XRD and the unsmoothed CGS data, there is a sharp transition across the film island edges. This transition from one slope regime to the

other is predicted by theory in Eqs. (9) and (10) and is due to the discontinuous film geometry as discussed in the previous section. By contrast, the smoothed CGS slope data completely miss this sharp transition by oversmoothing the raw interferogram.

The rather remarkable agreement between the raw CGS data and the XRD measurements provides a clear indication that CGS interferometry, if properly interpreted, can provide an excellent means of measuring deformations even at the presence of severe geometric discontinuities. It should be noted at this point that at the vicinity of the film-covered area, X-ray microdiffraction data were taken every 0.1 mm, which accounts for the high density of data reported in Fig. 10(*b*). A total of 940 measurements were taken across the wafer diameter. This measurement, although very spatially resolved, was very tedious and took a total of 3 h to complete. In contrast, the CGS measurement was almost instantaneous and was only limited by the acquisition time of the CCD camera used to record the interferograms.

The XRD and CGS slope data were also compared with theoretical predictions (Fig. 11), using the film stress as the single fitting parameter in Eq. (11). The comparison is quite good—for a given film stress, the shape and magnitude of the slope curve for XRD data, CGS data and theoretical prediction are all extremely close. This implies that even in the presence of strong curvature discontinuities of the type displayed in Fig. 5, plate theory does a remarkable job in capturing the wafer deformation behavior.

Conclusions

Coherent gradient sensing (CGS) interferometry provides a full-field, real-time, in situ slope and curvature measurement over the entire wafer surface. Nonuniform deformations have been measured using CGS interferometry in a partially covered film (island pattern). Highly resolved X-ray microdiffraction has been used to obtain slope and substrate curvature data from the same wafer for validation of the CGS measurement. Slope and curvature values measured from CGS interferometry are highly consistent with X-ray microdiffraction data and also with theoretical predictions of discontinuous curvature states.

References

[1] Rosakis, A. J., Singh, R. P., Tsuji, Y., Kolawa, E., and Moore, N. R., Jr., 1998, "Full-Field Measurements of Curvature Using Coherent Gradient Sensing: Application to Thin Film Characterization," Thin Solid Films, **325**(1-2), pp. 42–54.

[2] Lee, H., Rosakis, A. J., and Freund, L. B., 2001, "Full-Field Optical Measurement of Curvatures in Ultra-Thin-Film-Substrate Systems in the Range of Geometrically Nonlinear Deformations," J. Appl. Phys., **89**(11), pp. 6116–6129.

[3] Park, T. S., Suresh, S., Rosakis, A. J., and Ryu, J., 2003, "Measurement of Full-Field Curvature and Geometrical Instability of Thin Film-Substrate Systems Through CGS Interferometry," J. Mech. Phys. Solids, **51**(11-12), pp. 2191–2211.

[4] Freund, L. B., and Suresh, S., 2003, *Thin Film Materials*, Cambridge University Press, Cambridge, UK, Chaps. 2,3.

[5] Park, T. S., and Suresh, S., 2000, "Effects of Line and Passivation Geometry on Curvature Evolution During Processing and Thermal Cycling in Copper Interconnect Lines," Acta Mater., **48**(12), pp. 3169–3175.

[6] Park, T. S., Dao, M., Suresh, S., Rosakis, A. J., Pantuso, D., and Shankar, S., 2005, "Some Practical Issues of Curvature and Thermal Stress in Realistic Multi-level Metal Interconnect Structures," J. Electron. Mater. (submitted).

[7] Rosakis, A. J., Park, T. S., and Suresh, S., 2005, "Analytical and Numerical Modeling of Stress in Multi-level Interconnect Structures and Vias," Thin Solid Films (submitted).

[8] Rosakis, A. J., and Huang, Y., 2005, "A Thermoelastic Analysis of Film Stress and Non-Uniform Deformations in Wafers With Isolated and Periodic Film Islands" (unpublished).

[9] Tamura, N., MacDowell, A. A., Spolenak, R., Valek, B. C., Bravman, J. C., Brown, W. L., Celestre, R. S., Padmore, H. A., Batterman, B. W., and Patel, J. R., 2003, "Scanning X-Ray Microdiffraction With Submicrometer White Beam for Strain/Stress and Orientation Mapping in Thin Films," J. Synchrotron Radiat., **10**, pp. 137–143.

[10] Noyan, I. C., and Cohen, J. B., 1987, *Residual Stress*, Springer-Verlag, New York, Chap. 5.

[11] Gouldstone, A., Shen, Y.-L., Suresh, S., and Thompson, C. V., 1998, "Evolution of Stresses in Passivated and Unpassivated Metal Interconnects," J. Mater. Res., **13**(7), pp. 1956–1966.

[12] Stoney, G. G., 1909, "The Tension of Metallic Films Deposited by Electrolysis," Proc. R. Soc., London, **82**, pp. 172–175.